ACS OMEGA

http://pubs.acs.org/journal/acsodf

Article

Low-Temperature Direct Synthesis of Multilayered h-BN without Catalysts by Inductively Coupled Plasma-Enhanced Chemical Vapor Deposition

Masaya Yamamoto, Hiromasa Murata, Noriyuki Miyata, Hiroshi Takashima, Masayoshi Nagao, Hidenori Mimura, Yoichiro Neo, and Katsuhisa Murakami*

Cite This: *ACS Omega* 2023, 8, 5497−5505

Read Online

ACCESS | Metrics & More | Article Recommendations | Supporting Information

ABSTRACT: Low-temperature direct synthesis of thick multilayered hexagonal-boron nitride (h-BN) on semiconducting and insulating substrates is required to produce high-performance electronic devices based on two-dimensional (2D) materials. In this study, multilayered h-BN with a thickness exceeding 5 nm was directly synthesized on quartz and Si at low temperatures, between 400 and 500 °C, by inductively coupled plasma-enhanced chemical vapor deposition using borazine as the precursor material. The quality and thickness of the h-BN crystals were investigated with respect to synthesis parameters, namely, temperature, radio frequency power, N_2 flow rate, and H_2 flow rate. Introducing N_2 and H_2 carrier gases critically affected the deposition rate, and increasing the carrier gas flow rate enhanced the h-BN crystal quality. The typical optical band gap of synthesized h-BN was approximately 5.8 eV, consistent with that of previous studies. The full width at half-maximum of the h-BN Raman peak was 32−33 cm^{-1}, comparable to that of commercially available multilayered h-BN on Cu foil. These results are expected to facilitate the development of 2D materials for electronics applications.

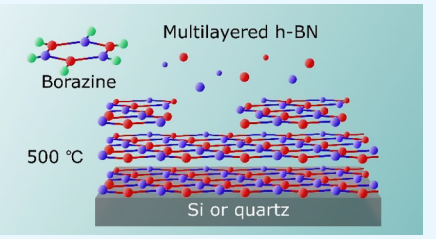

INTRODUCTION

In recent years, two-dimensional (2D) materials such as graphene have attracted considerable attention owing to their excellent properties. In particular, hexagonal-boron nitride (h-BN) is a 2D material with the following unique properties: resistance to high temperatures and chemical attack,[1] wide band gap,[1,2] high thermal conductivity,[3,4] and high lubricity,[5] which makes it suitable for several applications, including oxidant-resistant coating,[1,6,7] insulating layers,[8,9] deep ultraviolet (UV) sources,[10,11] and protective coating.[12,13] Moreover, h-BN has a flat surface on the atomic scale and no dangling bonds, and thus it is attractive as a substrate for 2D materials.[14−17]

Recently, we fabricated planar-type electron emission devices based on the graphene/h-BN/n-Si heterostructure.[18,19] The devices exhibit highly monochromatic electron emission from a flat surface, and the energy spread of the emission, based on the full width at half-maximum (FWHM), is 0.18 eV, which is better than that of a tungsten field emitter (0.3 eV) in a high-resolution electron microscope. The origin of this highly monochromatic electron emission is the suppression of electron inelastic scattering within the graphene/h-BN structure because both graphene and h-BN are composed of light elements. Thus, electronic devices with excellent properties can be achieved using 2D materials with high electron transmissivity. However, leakage current attributed to cracks in the h-BN layer formed during the transfer process from a Cu foil decreases the emission efficiency. Therefore, smooth multilayered h-BN without cracks and wrinkles on the Si substrate is required for further improvement of the electron emission properties of planar-type electron emission devices using the graphene/h-BN/Si heterostructure.

Recently, the synthesis of high-quality h-BN films on metal catalysts such as Cu,[20−22] Ni,[23,24] and Pt[25] substrates using borazine and ammonia borane as precursors has been reported. In the case of Pt and Cu substrates, growth of h-BN occurs via surface reactions on the catalytic substrate, resulting in monolayer h-BN. In contrast, growth of h-BN on the Ni substrate occurs via precipitation of oversaturated boron and nitrogen atoms from the Ni substrate during the cooling process. However, the solubility of boron atoms into Ni at high temperature is only 0.3%,[26] and nitrogen atoms are considered insoluble in Ni (~0.004%).[26] Therefore, because of the low and unbalanced solubility of boron and nitrogen atoms into the Ni substrate, it is difficult to synthesize multilayered h-BN with a thickness exceeding 5 nm and also with control of the thickness. In particular, the h-BN layer with a thickness range from 5 to 20 nm should be formed on a Si substrate at high reproducibility for the fabrication of our developed planar-type electron emission

Received: October 20, 2022
Accepted: January 12, 2023
Published: January 31, 2023

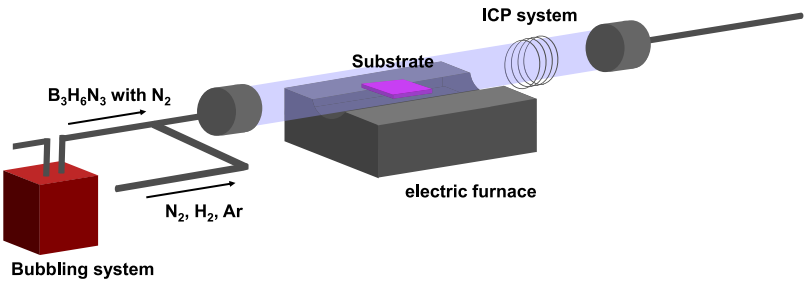

Figure 1. Schematic diagram of the ICP−CVD system.

Table 1. Details of Conditions for the Growth of h-BN

	temperature (°C)	RF power (W)	N_2 flow (sccm)	H_2 flow (sccm)	Ar flow (sccm)	pressure (Pa)	time (min)
Figure 4	300∼900	180	0	1	10	110	15
Figure 5	500	40∼180	5	10	0	10	15
Figure 6	500	180	0∼15	5	0	10	15
Figure 7	500	180	0	1∼10	0	110	15
Figure 8	500	180	15	10	0	10	5

devices using h-BN. In addition, high temperatures, i.e., exceeding 1000 °C for growth of h-BN on metal catalysts, and the time-consuming transfer process from metal catalysts are needed to fabricate the h-BN layer for electronic devices.[20−25] These factors limit the expansion of h-BN into industry and electronics applications. Thus, direct synthesis of multilayered h-BN on semiconducting and insulating substrates at low temperatures is important. One of the possible candidates for the synthesis of multilayered h-BN on an arbitral substrate at low temperature is atomic layer deposition (ALD).[27−31] ALD can atomically control the h-BN thickness and uniformity. However, their precursors of BCl_3 and NH_3 are highly toxic.[27−30] Therefore, the ALD system for h-BN growth requires high-cost safety and detoxification equipment. On the other hand, a low-cost and safe h-BN synthesis method is chemical vapor deposition (CVD) using borazine or ammonia borane as a precursor. There are several reports of the direct synthesis of h-BN using borazine or ammonia borane as precursors.[32−34] The mechanisms of direct growth of h-BN on the inert substrate have been described in previous papers.[33,34] The h-BN precursors such as borazine and ammonia borane are decomposed into boron and nitrogen species including ions, atoms, and radicals by plasma. These highly reactive species start the nucleation of the h-BN domain on the noncatalytic surface of the substrate. However, the effect of synthesis parameters on the quality of the resulting h-BN crystal has not yet been studied in detail.

In this study, we developed a method for the direct synthesis of multilayered h-BN using inductively coupled plasma−CVD (ICP−CVD) and investigated in detail the dependence of crystal quality on the following synthesis parameters: temperature, hydrogen flow rate, nitrogen flow rate, and input radio frequency (RF) power. Using this method with optimized growth conditions, we successfully synthesized multilayered h-BN (more than 50 nm) with comparable or better optical characteristics than that of commercially available multilayered h-BN on Cu foil.

EXPERIMENTAL SECTION

Growth of h-BN. Multilayered h-BN was directly synthesized on substrates using the originally developed ICP−CVD system shown in Figure 1. The radio frequency (RF, 13.56 MHz) coil for ICP generation was set on the outlet side of the electric furnace with respect to the direction of the carrier gas flow. Liquid borazine was used as the precursor of h-BN because of its stability of supply amount during the deposition process and low toxicity. Liquid borazine was stored at −10 °C and supplied to the CVD furnace by N_2 bubbling with a flow rate of 0.2 sccm. The base pressure before h-BN synthesis was evacuated to approximately 5×10^{-4} Pa using a turbo-molecular pump. Synthesis was performed on Si, SiO_2 (300 nm)/Si, and quartz substrates with a growth time of 15 min, followed by cooling to room temperature. The following growth parameters were varied as summarized in Table 1: flow rate of carrier gases ($Ar/N_2/H_2$), temperature, pressure, and RF plasma power.

The SiO_2(300 nm)/Si(100) substrate was cleaned with resist remover (STRIPPER-106, TOKYO OHKA KOGYO Co., LTD) at 80 °C, isopropyl alcohol, and ultrapure water. For the preparation of the Si (100) substrate, SiO_2 layers of the SiO_2/Si substrates cleaned in a previous manner were etched by a buffered hydrofluoric acid (BHF), and then the Si substrates were rinsed with ultrapure water. The quartz substrates were cleaned with isopropyl alcohol and deionized water. After the preparation of each substrate, three types of substrates were introduced into the ICP-CVD.

Material Characterization. Raman spectroscopy (Tokyo instrument Nanofiner 30) was performed using laser excitation at a wavelength of 488 nm and power of 7.9 mW for an exposure time of 3 min. Optical transmittance in the wavelength range of 185 to 800 nm was measured by UV and visible light absorption spectroscopy (Shimadzu UV-2600). Raman spectra of the h-BN layer were obtained from h-BN synthesized on a SiO_2/Si substrate since the h-BN/SiO_2/Si structure provides higher Raman signals of h-BN compared to the h-BN/Si structure. Therefore, the thinner h-BN layer can be evaluated by Raman spectroscopy using the h-BN/SiO_2/Si structure. It should be noted here that the substrate difference between Si and SiO_2/Si affects no dependence on the crystal quality of h-BN, which was confirmed by the Raman spectra of the thick h-BN synthesized on Si and SiO_2/Si substrate at the same time, as shown in Figure S1 of the Supporting Information. Transmittance spectra were obtained using h-BN synthesized on a quartz substrate. The thickness of h-BN was measured by multiwavelength ellipsometry with four light wavelengths: 450, 525, 595, and 660 nm (FilmSense FS-1) using the h-BN/Si structure, since a

https://doi.org/10.1021/acsomega.2c06757
ACS Omega 2023, 8, 5497−5505

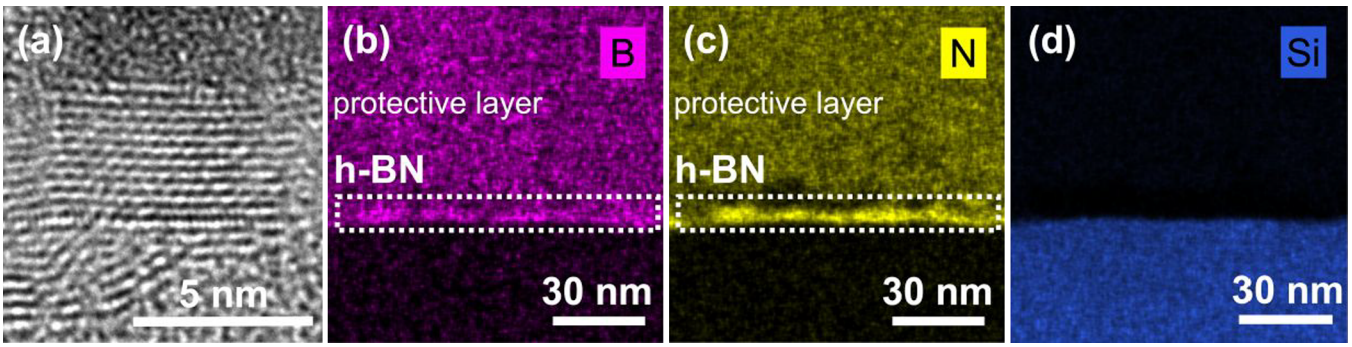

Figure 2. Characterization of the cross section of directly synthesized h-BN on the quartz substrate. The synthesis parameters were temperature of 500 °C, pressure of 10 Pa, RF input power of 180 W, N_2 flow rate of 15 sccm, H_2 flow rate of 5 sccm, and synthesis time of 15 min. (a) TEM image and STEM−EDS maps of (b) B, (c) N, and (d) Si elements.

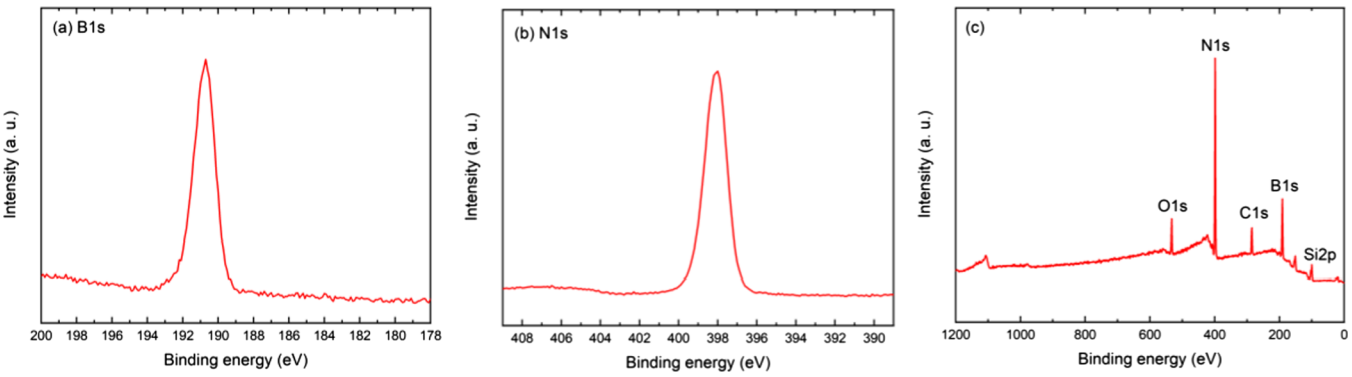

Figure 3. XPS (a) B1s, (b) N1s, and (c) survey spectra of the h-BN layer on the Si substrate. The synthesis parameters were temperature of 500 °C, pressure of 10 Pa, RF input power of 180 W, N_2 flow rate of 5 sccm, H_2 flow rate of 5 sccm, and synthesis time of 15 min.

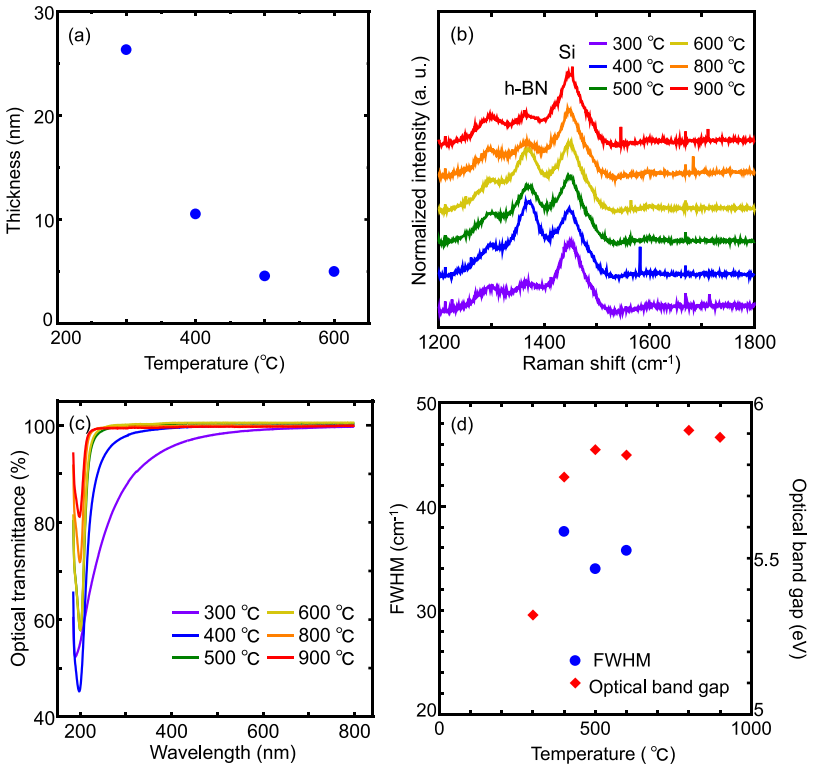

Figure 4. Effect of temperature on the thickness and optical properties of h-BN. (a) Thickness of h-BN as a function of temperature. (b) Raman and (c) transmittance spectra of h-BN. (d) FWHMs and optical band gaps of h-BN as a function of temperature.

https://doi.org/10.1021/acsomega.2c06757
ACS Omega 2023, 8, 5497−5505

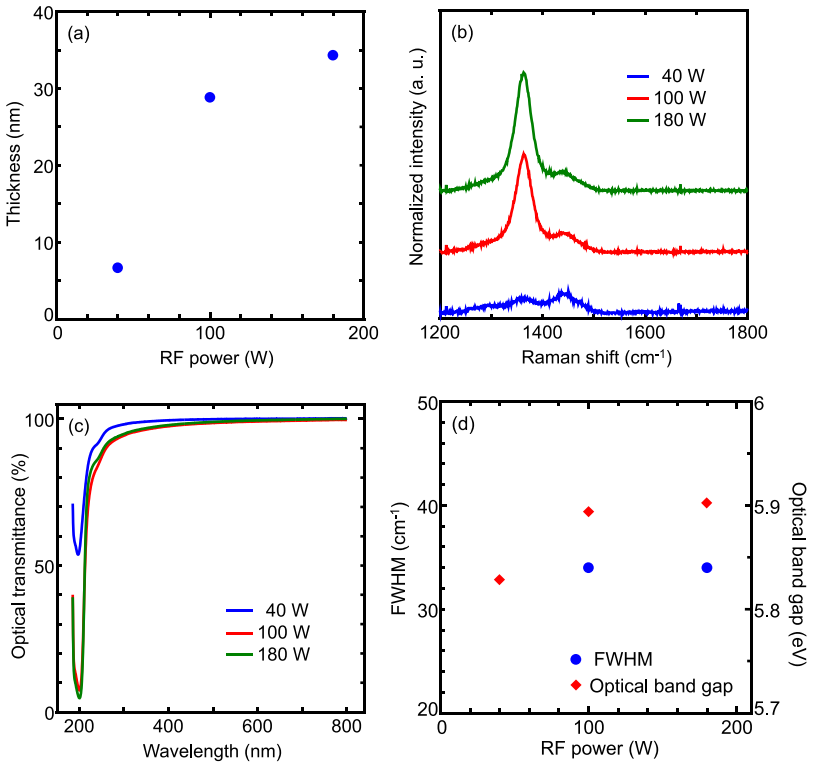

Figure 5. Effect of RF power on the thickness and optical properties of h-BN. (a) Thickness of h-BN as a function of RF power. (b) Raman and (c) transmittance spectra of h-BN. (d) FWHMs and optical band gaps of h-BN as a function of RF power.

simple structure model of h-BN on the Si substrate is the most suitable to measure the accurate film thickness of the h-BN layer by ellipsometry. X-ray photoelectron spectroscopy (XPS) analysis was performed with JOEL JSP-9200 using monochromatized Al Kα radiation ($h\upsilon$ = 1486.7 eV). Cross-sectional transmission electron microscopy (TEM) images and scanning TEM−energy-dispersive X-ray spectroscopy (STEM−EDS) mapping images of h-BN were observed with an FEI Tecnai Osiris operating at 200 kV.

Fabrication Processes of Capacitor Structures. The fabrication processes of the graphene/h-BN/Si capacitor structure are as follows. The SiO_2 (300 nm)/Si stack was used for the device fabrication. The capacitor area with a 10 μm × 10 μm square shape was patterned by photolithography and BHF wet etching of the SiO_2 layer. Then, multilayered h-BN with a thickness of around 10 nm was directly synthesized on the prepared substrate by ICP-CVD with a RF power of 180 W at 500 °C using borazine precursors. The topmost graphene electrode was directly synthesized on the h-BN layer by ICP-CVD with a RF power of 2 W at 800 °C using a mixture of Ar/CH_4(2.5%) gas with a pressure of 12 Pa for 1 h. The shape of the graphene/h-BN stack was patterned by photolithography, O_2 plasma etching of graphene, and SF_6 reactive ion etching of the h-BN layer. The contact electrode of the Ni(100 nm)/Ti(10 nm) stack was formed by photolithography, electron beam evaporation, and lift-off processes. The back contact electrode of the Ni(100 nm)/Ti(10 nm) stack was deposited on the backside of the Si substrate. The same capacitor structure using the multilayered h-BN transferred from a Cu foil was also fabricated for comparison of the electrical characterization of h-BN. The detailed fabrication processes of the capacitor structure were described in ref 18.

RESULTS AND DISCUSSION

Figure 2a shows the cross-sectional TEM image of h-BN directly grown on the quartz substrate. The layered structure, a feature of 2D materials, was clearly observed. The interlayer distance was approximately 0.35 nm, consistent with a previously reported value for h-BN.[23] Figure 2b−d shows the STEM−EDS maps of boron, nitrogen, and Si elements, revealing that boron and nitrogen elements were localized only on the top of the quartz surface.

Figure 3a−c shows the XPS spectra of h-BN directly synthesized on the Si substrate. The binding energies of B1s and N1s, measured from the spectra shown in Figure 3a,b, were 190.7 and 398.1 eV, respectively. These values are in good agreement with reported values.[23−25] The N/B ratio of synthesized h-BN calculated from the XPS spectra was approximately 1.1, which corresponded to the stoichiometric ratio of h-BN. The survey spectrum (Figure 3c) contained O_{1s} and C_{1s} peaks because h-BN was exposed to air after growth. The results of TEM and XPS analyses verified that h-BN was successfully grown.

Figure 4a−d shows the thickness and optical properties of h-BN grown at different temperatures. Other growth parameters are shown in Table 1. The thickness of h-BN decreased with increasing temperature, as shown in Figure 4a. In the case of high growth temperature, borazine should decompose on the upstream side of the electric furnace, and thus borazine cannot reach the substrate. In fact, a brown contaminant was confirmed on the upstream side of the electric furnace at growth temperatures exceeding 500 °C. In addition, the roughness of the Si substrate increased when the synthesis temperature was greater than 800 °C, and thus it was difficult to measure the thickness of the h-BN layer by multiwavelength ellipsometry. Figure 4b shows the Raman spectra of h-BN synthesized on the

https://doi.org/10.1021/acsomega.2c06757
ACS Omega 2023, 8, 5497−5505

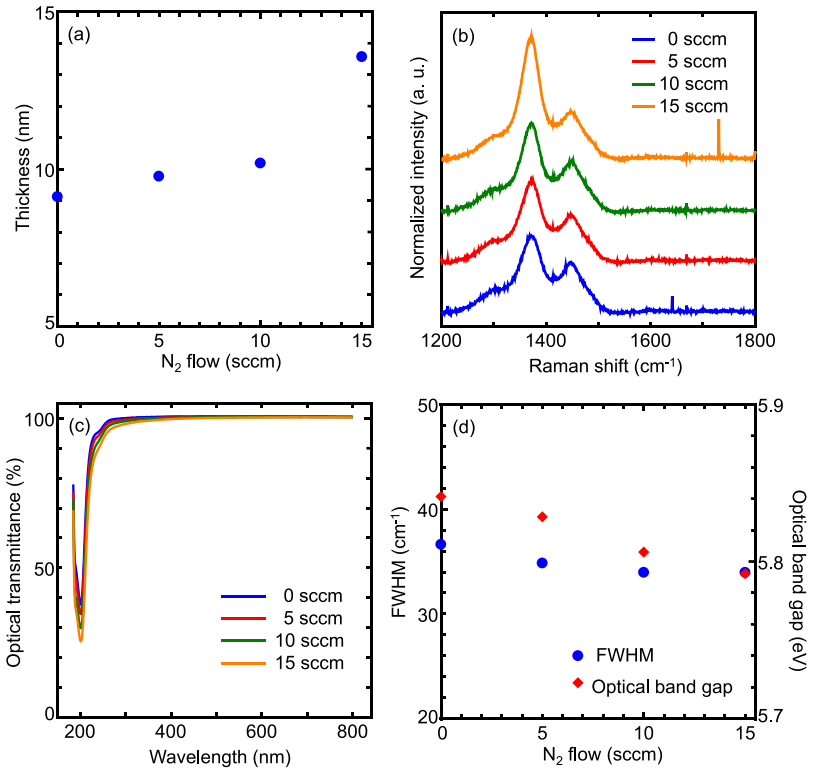

Figure 6. Effect of N_2 flow rate on the thickness and optical properties of h-BN. (a) Thickness of h-BN as a function of N_2 flow rate. (b) Raman and (c) transmittance spectra of h-BN. (d) FWHMs and optical band gaps of h-BN as a function of N_2 flow rate.

SiO_2/Si substrate at different growth temperatures. The optical images of the h-BN layer with different thickness corresponding to Figure 4b are also shown in Figure S2 of the Supporting Information. The samples showed a homogeneous color contrast. The thickest samples with a thickness of around 26 nm synthesized at 300 °C showed blue color. The peaks at approximately 1372 and 1450 cm^{-1} correspond to the E^{2g} phonon vibration of h-BN and the third-order transverse optical phonon mode of Si in the SiO_2/Si substrate, respectively.[34] The intensity of the h-BN peak was normalized using the intensity of the Si peak at 1450 cm^{-1} in this study. The h-BN peak was not observed at low (300 °C) and high temperatures, i.e., greater than 800 °C. At high temperatures, the intensity of Raman scattered light from h-BN is very low because the h-BN layer is thin, and thus the h-BN peak cannot be observed. In contrast, low growth temperatures (e.g., 300 °C) promote the formation of amorphous-like BN, which is not transparent but brownish. These results were supported by the transmittance spectra of h-BN/quartz, as shown in Figure 4c. Interestingly, the transmittance spectrum at 300 °C showed that h-BN absorbed visible light, which suggested that the optical properties of the materials synthesized at 300 °C are different from h-BN. In fact, in the case of the synthesis temperature of above 400 °C, the values of the optical transmittance at around 200 nm decreases with the thickness of h-BN. However, optical transmittance at around 200 nm for synthesis temperature of 300 °C is higher than that of 400 °C even though the thickness synthesized at 300 °C is thicker than that at 400 °C. Figure 4d shows the optical band gap of h-BN and the FWHM of the Raman peak arising from the E^{2g} phonon vibration of h-BN as a function of the growth temperature. The optical band gap was calculated using Tauc's equation.[34] From the optical transmission spectra, the optical band gap of h-BN synthesized at and above the temperature of 400 °C was in the range of 5.76 to 5.91 eV, consistent with a previously reported optical band gap of h-BN (5.9 eV).[20,22,23] It is worth noting here that the optical band gap can be obtained from h-BN synthesized at high temperature of greater than 800 °C, and these values were highest of around 5.91 eV. This result indicate that h-BN layer was grown at the high temperature of more than 800 °C even though the Raman signal was not observed due to the very thin film thickness. In contrast, the optical band gap of h-BN grown at a temperature of 300 °C was lower than 5.31 eV, suggesting that disordered amorphous-like BN was deposited at a growth temperature of 300 °C. The lowest value of the FWHM of the h-BN Raman peak was approximately 34.0 cm^{-1}, which was obtained from the spectrum of h-BN grown at 500 °C. Therefore, 500 °C was adopted as the optimal growth temperature. It should be noted here that Ar gas of 10 sccm was used in the experiment for synthesis temperature dependence. We also confirmed the influence of Ar on h-BN synthesis as shown in Figure S3 of the Supporting Information. The h-BN thickness decreased with the increase of the Ar flow rate. The optical band gap and FWHM of the Raman peak of h-BN were almost constant with and without Ar flow. Therefore, to reduce the synthesis parameters of ICP-CVD and become simpler, we eliminated the Ar flow from next experiments.

Figure 5a–d shows the dependence of the thickness and optical properties of directly grown h-BN on the RF input power. Other growth parameters are shown in Table 1. The thickness increased with increasing RF input power and reached approximately 34 nm at a RF power of 180 W, as shown in Figure 5a. Figure 5b shows the Raman spectra of h-BN synthesized on the SiO_2/Si substrate at different RF powers. The Raman peak at approximately 1372 cm^{-1} attributed to h-BN was observed when h-BN was grown at the RF input powers of 100

https://doi.org/10.1021/acsomega.2c06757
ACS Omega 2023, 8, 5497−5505

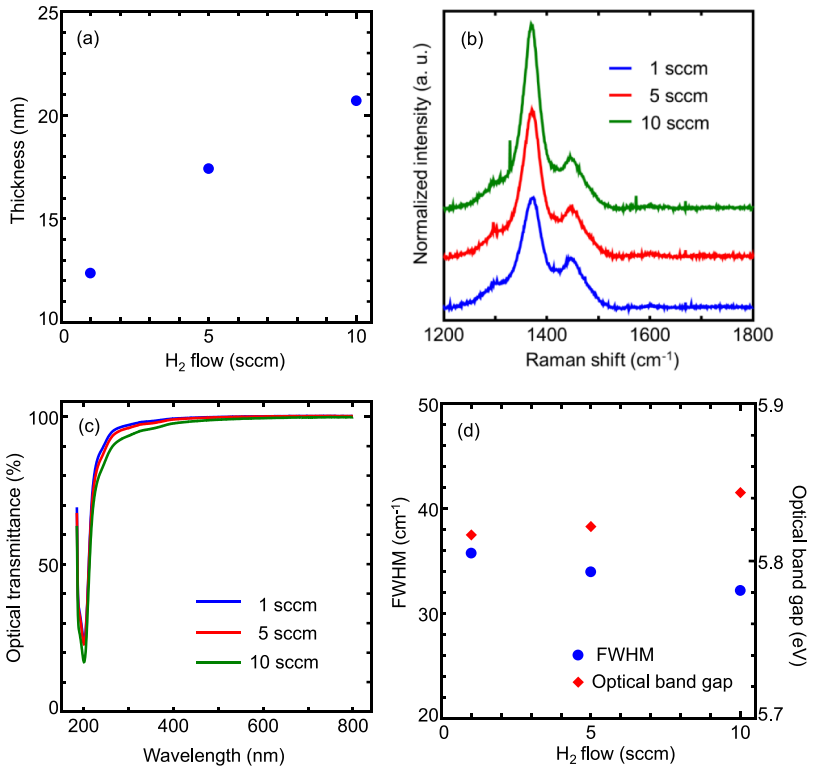

Figure 7. Effect of the H_2 flow rate on the thickness and optical properties of h-BN. (a) Thickness of h-BN as a function of H_2 flow rate. (b) Raman and (c) transmittance spectra of h-BN. (d) FWHMs and optical band gaps of h-BN as a function of H_2 flow rate.

and 180 W. However, h-BN Raman peaks were not detected when h-BN was synthesized at a RF input power of 40 W, possibly because the thin (6 nm) h-BN layer reduced the intensity of Raman scattered light. All samples had absorption at light of approximately 200 nm in wavelength, as shown in the optical transmittance spectra of h-BN (Figure 5c). Transmittance at approximately 200 nm was higher for h-BN synthesized at 40 W than for h-BN synthesized at 100 and 180 W, further indicating that the h-BN layer grown at 40 W was thinner than that grown at 100 and 180 W. Figure 5d shows the optical band gaps obtained from the optical transmittance spectra and the FWHM of the Raman peak of h-BN as a function of RF power. Although these values were almost equivalent for h-BN grown at 100 and 180 W, the h-BN layer grown at 180 W was thicker than that grown at 100 W. Thus, 180 W was adopted as the optimal RF input power.

Figure 6a–d shows the thickness and optical properties of directly grown h-BN as a function of the N_2 gas flow rate. Other growth parameters are shown in Table 1. Although the effect of the N_2 gas flow rate on h-BN was initially investigated at a constant pressure of 110 Pa, the deposition rate of greater than 3.4 nm/min corresponding to a thickness exceeding 50 nm at 15 min was too fast for the fabrication processes of our electron emission devices. Hence, the synthesis pressure was reduced to 10 Pa to decrease the partial pressure of borazine. The h-BN thickness increased with increasing N_2 gas flow rate, as shown in Figure 6a. The Raman spectra of h-BN synthesized on the SiO_2/Si substrate at all N_2 gas flow rates showed a peak at approximately 1372 cm^{-1} attributed to h-BN, as shown in Figure 6b. The intensity of the h-BN peak with respect to the intensity of the Si peak at approximately 1450 cm^{-1} increased with increasing N_2 flow rate, attributed to the increasing thickness of the h-BN layer. This tendency was also supported by the transmission spectra of h-BN shown in Figure 6c. Transmittance at approximately 200 nm decreased with increasing N_2 flow rate. These results suggest that the growth rate of h-BN under our experimental conditions is determined by the rate of supply of nitrogen atoms. Figure 6d shows the optical band gaps obtained from the optical transmittance spectra and the FWHM of the Raman peak of h-BN as a function of the N_2 flow rate. The optical band gap slightly decreased with increasing N_2 flow, probably owing to the layer–layer interaction promoted by the increased thickness.[33] However, the difference was very small (i.e., 5.79 to 5.84 eV), and the optical band gaps were consistent with previously reported values.[20,22,23] The FWHM of the h-BN Raman peak also decreased with increasing N_2 flow rate and reached approximately 34.0 cm^{-1} at the N_2 flow rates of 10 and 15 sccm. From these results, the optimal N_2 flow rate for our experimental setup was determined to be 15 sccm.

Figure 7a–d shows the effect of the H_2 flow rate on the thickness and optical properties of directly grown h-BN. Other growth parameters are shown in Table 1. The thickness of the h-BN layer increased with increasing H_2 gas flow rate, as shown in Figure 7a. This suggests that the h-BN precursor can easily reach the substrate when H_2 gas is introduced. When H_2 gas was added, contaminants from the decomposition of borazine were not observed on the upstream side of the electric furnace with respect to the direction of the carrier gas flow, although these contaminants were detected under other experimental conditions without adding H_2 gas. Figure 7b shows the Raman spectra of h-BN synthesized on the SiO_2/Si substrate at different H_2 gas flow rates. The h-BN Raman peak was observed for h-BN synthesized at all H_2 flow rates. By increasing the H_2 flow rate, the intensity of the h-BN Raman peak increased. Transmittance at approximately 200 nm slightly decreased with increasing H_2

https://doi.org/10.1021/acsomega.2c06757
ACS Omega 2023, 8, 5497−5505

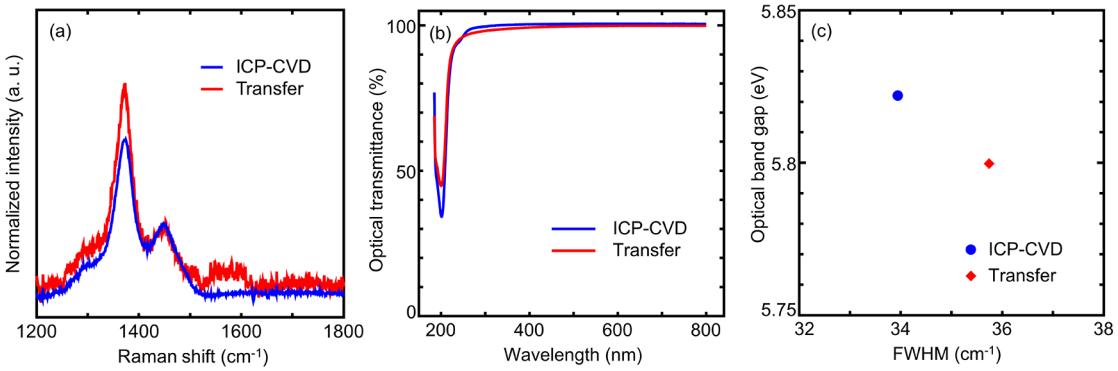

Figure 8. (a) Raman spectra, (b) transmittance spectra, and (c) FWHMs and optical band gaps of h-BN synthesized by ICP−CVD under the optimized conditions and h-BN synthesized on Cu foil.

flow rate, as shown in Figure 7c, reflecting the increase in the thickness of the h-BN layer. Figure 7d shows the optical band gaps obtained from the optical transmittance spectra and the FWHM of the Raman peak of h-BN as a function of the H_2 flow rate. The optical band gap was in the range of 5.82 of 5.84 eV, close to ideal values, and slightly increased with increasing H_2 flow. The FWHM of the h-BN Raman peak decreased with increasing H_2 flow rate and reached 32 cm^{-1} at the H_2 flow rate of 10 sccm. From these results, the optimal H_2 flow rate in our experimental setup was determined to be 10 sccm.

From the above analysis, it was revealed that increasing the H_2 and N_2 flow rates led to an increase in the thickness and quality of the h-BN layer. We also confirmed that the synthesis pressure affects the thickness of h-BN. The thickness of h-BN increases with synthesis pressure, as shown in Table S1 of the Supporting Information. However, the optical bandgap and crystal quality (i.e., FWHM of Raman spectra of h-BN) were almost constant. In our target application of the planar-type electron emission devices, h-BN thickness of around 10 nm is required. As considered the controllability of the h-BN thickness in our device applications, we selected the low pressure of 10 Pa for h-BN synthesis conditions. Therefore, the optimal synthesis conditions of h-BN in our experimental setup were decided as a synthesis temperature of 500 °C, RF input power of 180 W, synthesis pressure of 10 Pa, N_2 flow rate of 15 sccm, and H_2 flow rate of 10 sccm. We synthesized h-BN directly on the SiO_2/Si and quartz substrates under the optimized conditions for 5 min, obtaining h-BN layers of 9 nm in thickness, similar to the thickness of commercially available multilayered h-BN on Cu foil (EM Japan Co., Ltd. Cat No. G-53). h-BN synthesized on Cu foil was transferred to quartz and SiO_2/Si from the Cu foil following the technique described in ref 18. Figure 8a−c shows the Raman spectra, transmittance spectra, and Raman peak FWHMs and optical band gaps of h-BN synthesized by ICP−CVD under the optimized conditions and h-BN synthesized on Cu foil. These results indicate that we succeeded in directly synthesizing h-BN with comparable or better optical characteristics than commercially available multilayered h-BN on Cu foil.

Figure 9 shows the typical current−voltage curves of the capacitor device using the graphene/h-BN/Si heterostructure. The leakage current level of directly synthesized h-BN is lower than that of the transferred h-BN. This is due to the smooth surface of the directly synthesized h-BN without any cracks and wrinkles, which is confirmed by scanning electron microscopy observations as shown in Figure S4 of the Supporting Information.

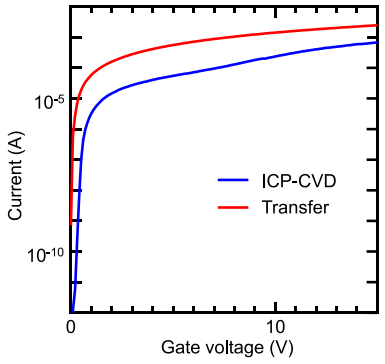

Figure 9. Current−voltage curves of the graphene/h-BN/Si capacitor structure using multilayered h-BN directly synthesized by ICP-CVD and transferred from a Cu foil.

CONCLUSIONS

In this study, h-BN was directly synthesized on semiconducting and insulating substrates at low temperatures, i.e., from 400 to 500 °C, by ICP−CVD using borazine as the precursor material. The layered structure of h-BN was observed by cross-sectional TEM. The N/B atomic ratio of synthesized h-BN analyzed by XPS was approximately 1.1, which agreed with the stoichiometric ratio of h-BN. The role of N_2 and H_2 gases in the growth of h-BN was elucidated in detail by investigating the effect of carrier gas flow rate and species on the thickness and optical properties of synthesized h-BN. These findings made it possible to directly synthesize h-BN without using catalysts, and synthesized h-BN had comparable or better optical properties than commercially available multilayered h-BN on Cu foil. In addition, directly synthesized multilayered h-BN had a thickness exceeding 5 nm, which is commonly difficult to obtain with CVD using metal catalysts. The findings of this study can promote the development of highly monochromatic electron emission devices using the graphene/h-BN/Si heterostructure and, furthermore, are expected to contribute to the direct synthesis of h-BN at low temperatures and the expansion of h-BN into industrial applications.

ASSOCIATED CONTENT

Supporting Information

The Supporting Information is available free of charge at https://pubs.acs.org/doi/10.1021/acsomega.2c06757.

Raman spectra of h-BN directly synthesized on Si and SiO_2 substrate at the same synthesis condition are shown

https://doi.org/10.1021/acsomega.2c06757
ACS Omega 2023, 8, 5497−5505

in Figure S1; optical images of h-BN layer on SiO_2/Si substrate synthesized at different growth temperature are shown in Figure S2; effect of the Ar flow rate on the thickness and optical properties of h-BN is shown in Figure S3; SEM images of multilayered h-BN directly synthesized on the Si substrate are shown in Figure S4; synthesis pressure dependence of thickness, FWHM of Raman peak, and optical bandgap of h-BN are summarized in Table S1 (PDF).

AUTHOR INFORMATION

Corresponding Author

Katsuhisa Murakami − *National Institute of Advanced Industrial Science and Technology, Tsukuba, Ibaraki 305-8568, Japan;* orcid.org/0000-0001-5999-5581; Email: murakami.k@aist.go.jp

Authors

Masaya Yamamoto − *Research Institute of Electronics, Shizuoka University, Hamamatsu, Shizuoka 432-8011, Japan; National Institute of Advanced Industrial Science and Technology, Tsukuba, Ibaraki 305-8568, Japan*

Hiromasa Murata − *National Institute of Advanced Industrial Science and Technology, Tsukuba, Ibaraki 305-8568, Japan;* orcid.org/0000-0002-7136-8131

Noriyuki Miyata − *National Institute of Advanced Industrial Science and Technology, Tsukuba, Ibaraki 305-8568, Japan;* orcid.org/0000-0003-0964-2694

Hiroshi Takashima − *National Institute of Advanced Industrial Science and Technology, Tsukuba, Ibaraki 305-8568, Japan;* orcid.org/0000-0002-3437-468X

Masayoshi Nagao − *National Institute of Advanced Industrial Science and Technology, Tsukuba, Ibaraki 305-8568, Japan*

Hidenori Mimura − *Research Institute of Electronics, Shizuoka University, Hamamatsu, Shizuoka 432-8011, Japan*

Yoichiro Neo − *Research Institute of Electronics, Shizuoka University, Hamamatsu, Shizuoka 432-8011, Japan;* orcid.org/0000-0003-1988-8292

Complete contact information is available at: https://pubs.acs.org/10.1021/acsomega.2c06757

Notes

The authors declare no competing financial interest.

ACKNOWLEDGMENTS

This work was partly supported by JSPS KAKENHI Grant Numbers JP18H01505, JP21K01401, JP22K18800, and JP22K18855. The authors are indebted to Mr. N. Saitoh (AIST) for the cross-sectional TEM observations. We thank Edanz (https://jp.edanz.com/ac) for editing a draft of this manuscript.

REFERENCES

(1) Li, L. H.; Cervenka, J.; Watanabe, K.; Taniguchi, T.; Chen, Y. Strong Oxidation Resistance of Atomically Thin Boron Nitride Nanosheets. *ACS Nano* **2014**, *8*, 1457−1462.

(2) Zhang, K.; Feng, Y.; Wang, F.; Yang, Z.; Wang, J. Two dimensional hexagonal boron nitride (2D-hBN): synthesis, properties and applications. *J. Mater. Chem. C* **2017**, *5*, 11992−12022.

(3) Jo, I.; Pettes, M. T.; Kim, J.; Watanabe, K.; Taniguchi, T.; Yao, Z.; Shi, L. Thermal Conductivity and Phonon Transport in Suspended Few-Layer Hexagonal Boron Nitride. *ACS Nano* **2013**, *13*, 550−554.

(4) Meng, W.; Huang, Y.; Fu, Y.; Wang, Z.; Zhi, C. Polymer composites of boron nitride nanotubes and nanosheets. *J. Mater. Chem. C* **2014**, *2*, 10049−10061.

(5) Kimura, Y.; Wakabayashi, T.; Okada, K.; Wada, T.; Nishikawa, H. Boron nitride as lubricant additive. *Wear* **1999**, *232*, 199−206.

(6) Liu, Z.; Gong, Y.; Zhou, W.; Ma, L.; Yu, J.; Idrobo, J. C.; Jung, J.; MacDonald, A. H.; Vajtai, R.; Lou, J.; Ajayan, P. M. Ultrathin HighTemperature Oxidation-Resistant Coatings of Hexagonal Boron Nitride. *Nat. Commun.* **2013**, *4*, 2541.

(7) Matsumoto, N.; Takao, Y.; Nagao, M.; Murakami, K. Oxidation Resistance Improvement of Graphene-Oxide-Semiconductor Planar-Type Electron Sources Using h-BN as an Oxygen-Resistant, Electron-Transmissive Coating. *ACS Omega* **2022**, *7*, 33004−33009.

(8) Hattori, Y.; Taniguchi, T.; Watanabe, K.; Nagashio, K. Layer-by-Layer Dielectric Breakdown of Hexagonal Boron Nitride. *ACS Nano* **2015**, *9*, 916−921.

(9) Knobloch, T.; Illarionov, Y. Y.; Ducry, F.; Schleich, C.; Wachter, S.; Watanabe, K.; Taniguchi, T.; Mueller, T.; Waltl, M.; Lanza, M.; Vexler, M. I.; Luisier, M.; Grasser, T. The performance limits of hexagonal bron nitride as an insulator for scaled CMOS devices based on two-dimensional materials. *Nat. Electron.* **2021**, *4*, 98−108.

(10) Watanabe, K.; Taniguchi, T.; Kanda, H. Direct-Bandgap Properties and Evidence for Ultraviolet Lasing of Hexagonal Boron Nitride Single Crystal. *Nat. Mater.* **2004**, *3*, 404−409.

(11) Kubota, Y.; Watanabe, K.; Tsuda, O.; Taniguchi, T. Deep Ultraviolet Light−Emitting Hexagonal Boron Nitride Synthesized at Atmospheric Pressure. *Science* **2007**, *317*, 932−934.

(12) Husain, E.; Narayanan, T. N.; Taha-Tijerina, J. J.; Vinod, S.; Vajtai, R.; Ajayan, P. M. Marine Corrosion Protective Coatings of Hexagonal Boron Nitride Thin Films on Stainless Steel. *ACS Appl. Mater. Interfaces* **2013**, *5*, 4129−4135.

(13) Jia, S.; Chen, W.; Zhang, J.; Lin, C. -Y.; Guo, H.; Lu, G.; Li, K.; Zhai, T.; Ai, Q.; Lou, J. CVD growth of high-quality and large-area continuous h-BN thin films directly on stainless-steel as protective coatings. *Mater. Today Nano* **2021**, *16*, No. 100135.

(14) Dean, C. R.; Young, A. F.; Meric, I.; Lee, C.; Wang, L.; Sorgenfrei, S.; Watanabe, K.; Taniguchi, T.; Kim, P.; Shepard, K. L.; Hone, J. Boron Nitride Substrates for High-Quality Graphene Electronics. *Nat. Nanotechnol.* **2010**, *5*, 722−726.

(15) Gannett, W.; Regan, W.; Watanabe, K.; Taniguchi, T.; Crommie, M. F.; Zettl, A. Boron Nitride Substrates for High Mobility Chemical Vapor Deposited Graphene. *Appl. Phys. Lett.* **2011**, *98*, No. 242105.

(16) Lee, G.-H.; Yu, Y.-J.; Cui, X.; Petrone, N.; Lee, C.-H.; Choi, M. S.; Lee, D.-Y.; Lee, C.; Yoo, W. J.; Watanabe, K.; Taniguchi, T.; Nuckolls, C.; Kim, P.; Hone, J. Flexible and Transparent MoS_2 Field-Effect Transistors on Hexagonal Boron Nitride-Graphene Heterostructures. *ACS Nano* **2013**, *7*, 7931−7936.

(17) Xu, S.; Wu, Z.; Lu, H.; Han, Y.; Long, G.; Chen, X.; Han, T.; Ye, W.; Wu, Y.; Lin, J.; Shen, J.; Cai, Y.; He, Y.; Zhang, F.; Lortz, R.; Cheng, C.; Wang, N. Universal Low-Temperature Ohmic Contacts for Quantum Transport in Transition Metal Dichalcogenides. *2D Mater.* **2016**, *3*, No. 021007.

(18) Murakami, K.; Igari, T.; Mitsuishi, K.; Nagao, M.; Sasaki, M.; Yamada, Y. Highly Monochromatic Electron Emission from Graphene/Hexagonal Boron Nitride/Si Heterostructure. *ACS Appl. Mater. Interfaces* **2020**, *12*, 4061−4067.

(19) Igari, T.; Nagao, M.; Mitsuishi, K.; Sasaki, M.; Yamada, Y.; Murakami, K. Origin of Monochromatic Electron Emission From Planar-Type Graphene/h-BN/n-Si Devices. *Phys. Rev. Appl.* **2021**, *15*, No. 014044.

(20) Song, X.; Gao, J.; Nie, Y.; Gao, T.; Sun, J.; Ma, D.; Li, Q.; Chen, Y.; Jin, C.; Bachmatiuk, A.; Rümmeli, M. H.; Ding, F.; Zhang, Y.; Liu, Z. Chemical vapor deposition growth of large-scale hexagonal boron nitride with controllable orientation. *Nano Res.* **2015**, *8*, 3164−3176.

(21) Stehle, Y.; Meyer, H. M.; Unocic, R. R.; Kidder, M.; Polizos, G.; Datskos, P. G.; Jackson, R.; Smirnov, S. N.; Vlassiouk, I. V. Synthesis of Hexagonal Boron Nitride Monolayer: Control of Nucleation and Crystal Morphology. *Chem. Mater.* **2015**, *27*, 8041−8047.

(22) Wu, Q.; Park, J.-H.; Park, S.; Jung, S. J.; Suh, H.; Park, N.; Wongwiriyapan, W.; Lee, S.; Lee, Y. H.; Song, Y. J. Single Crystalline Film of Hexagonal Boron Nitride Atomic Monolayer by Controlling Nucleation Seeds and Domains. *Sci. Rep.* **2015**, *5*, 16159.
(23) Shi, Y.; Hamsen, C.; Jia, X.; Kim, K. K.; Reina, A.; Hofmann, M.; Hsu, A. L.; Zhang, K.; Li, H.; Juang, Z.-Y.; Dresselhaus, M. S.; Li, L.-J.; Kong, J. Synthesis of Few-Layer Hexagonal Boron Nitride Thin Film by Chemical Vapor Deposition. *ACS Nano* **2010**, *10*, 4134−4139.
(24) Taslim, A. B.; Nakajima, H.; Lin, Y.-C.; Uchida, Y.; Kawahara, K.; Okazaki, T.; Suenaga, K.; Hibino, H.; Ago, H. Synthesis of sub-millimeter single-crystal grains of aligned hexagonal boron nitride on an epitaxial Ni film. *Nanoscale* **2019**, *11*, 14668−14675.
(25) Park, J.-H.; Park, J. C.; Yun, S. J.; Kim, H.; Luong, D. H.; Kim, S. M.; Choi, S. H.; Yang, W.; Kong, J.; Kim, K. K.; Lee, Y. H. Large-Area Monolayer Hexagonal Boron Nitride on Pt Foil. *ACS Nano* **2014**, *8*, 8520−8528.
(26) Suzuki, S.; Pallares, R. M.; Hibino, H. Growth of atomically thin hexagonal boron nitride films by diffusion through a metal film and precipitation. *J. Phys. D: Appl. Phys.* **2012**, *45*, No. 385304.
(27) Driver, M. S.; Beatty, J. D.; Olanipekun, O.; Reid, K.; Rath, A.; Voyles, P. M.; Kelber, J. A. Atomic Layer Epitaxy of h-BN(0001) Multilayers on Co(0001) and Molecular Beam Epitaxy Growth of Graphene on h-BN(0001)/Co(0001). *Langmuir* **2016**, *32*, 2601−2607.
(28) Jones, J.; Beauclair, B.; Olanipekun, O.; Lightbourne, S.; Zhang, M.; Pollok, B.; Pilli, A.; Kelber, J. Atomic layer deposition of h-BN(0001) and RuO_2(110)/Ru(0001). *J. Vac. Sci. Technol., A* **2017**, *35*, No. 01B139.
(29) Pilli, A.; Jones, J.; Chugh, N.; Kelber, J.; Pasquale, F.; LaVoie, A. Atomic layer deposition of BN as a novel capping barrier for B_2O_3. *J. Vac. Sci. Technol. A* **2019**, *37*, No. 041505.
(30) Jones, J.; Pilli, A.; Lee, V.; Beatty, J.; Beauclair, B.; Chugh, N.; Kelber, J. Atomic layer deposition of h-BN(0001) multilayers on Ni(111) and chemical vapor deposition of graphene on h-BN(0001)/Ni(111). *J. Vac. Sci. Technol., A* **2019**, *37*, No. 060903.
(31) Rajendran, S.; Pilli, A.; Omolere, O.; Kelber, J.; Arava, L. M. R. An All-Solid-State Battery with a Tailored Electrode-Electrolyte Interface Using Surface Chemistry and Interlayer-Based Approaches. *Chem. Mater.* **2021**, *33*, 3401−3412.
(32) Tay, R. Y.; Tsang, S. H.; Loeblein, M.; Chow, W. L.; Loh, G. C.; Toh, J. W.; Ang, S. L.; Teo, E. H. T. Direct growth of nanocrystalline hexagonal boron nitride films on dielectric substrates. *Appl. Phys. Lett.* **2015**, *106*, No. 101901.
(33) Behura, S.; Nguyen, P.; Che, S.; Debbarma, R.; Berry, V. Large-Area, Transfer-Free, Oxide-Assisted Synthesis of Hexagonal Boron Nitride Films and Their Heterostructures with MoS_2 and WS_2. *J. Am. Chem. Soc.* **2015**, *137*, 13060−13065.
(34) Liu, D.; Chen, X.; Yan, Y.; Zhang, Z.; Jin, Z.; Yi, K.; Zhang, C.; Zheng, Y.; Wang, Y.; Yang, J.; Xu, X.; Chen, J.; Lu, Y.; Wei, D.; Wee, A. T. S.; Wei, D. Conformal hexagonal-boron nitride dielectric interface for tungsten diselenide devices with improved mobility and thermal dissipation. *Nat. Commun.* **2019**, *10*, 1188.

https://doi.org/10.1021/acsomega.2c06757
ACS Omega 2023, 8, 5497−5505